Q. J. R. Meteorol. Soc. (2005), **1xx**, pp. 1–999

Construction of covariance functions with variable length fields

By Gregory Gaspari[1,2], Stephen E. Cohn[2], Jing Guo[1,2], and Steven Pawson[2] *

[1] *Science Applications International Corporation, Beltsville, MD 20705, USA.*
[2] *Global Modeling and Assimilation Office, Code 900.3, NASA/Goddard Space Flight Center, Greenbelt, MD 20771, USA.*

SUMMARY

This article focuses on construction, directly in physical space, of three-dimensional covariance functions parametrized by a tunable length field, and on an application of this theory to reproduce the Quasi-Biennial Oscillation (QBO) in the Goddard Earth Observing System, Version 4 (GEOS-4) data assimilation system. These covariance models are referred to as *multi-level* or *nonseparable*, to associate them with the application where a multi-level covariance with a large troposphere to stratosphere length field gradient is used to reproduce the QBO from sparse radiosonde observations in the tropical lower stratosphere. The multi-level covariance functions extend well-known single-level covariance functions depending only on a length scale. Generalizations of the first- and third-order autoregressive covariances in three dimensions are given, providing multi-level covariances with zero and three derivatives at zero separation, respectively. Multi-level piecewise rational covariances with two continuous derivatives at zero separation are also provided. Multi-level powerlaw covariances are constructed with continuous derivatives of all orders. Additional multi-level covariance functions are constructed using the Schur product of single- and multi-level covariance functions. A multi-level powerlaw covariance used to reproduce the QBO in GEOS-4 is described along with details of the assimilation experiments. The new covariance model is shown to represent the vertical wind shear associated with the QBO much more effectively than in the baseline GEOS-4 system.

KEYWORDS: Data assimilation Correlation functions nonseparable Quasi-Biennial Oscillation

1 INTRODUCTION

This article focuses on constructive development and application of covariance functions with length scales determined by certain prescribed functions. These reduce to covariance functions, depending only on a length scale, that have been widely applied in diverse applications where covariance models are required. Covariance modeling applications in the earth sciences are emphasized, where correlation length scales vary in altitude and/or on horizontal surfaces. In accordance with standard terminology, these covariance functions will be said to depend on a variable *length field* (cf. Yaglom 1987, p. 19).

Parametrized forecast- and observation-error covariance function models depending on a length field have been an important component of atmospheric data assimilation

* Corresponding author: Gregory Gaspari, Code 900.3, NASA/Goddard Space Flight Center, Greenbelt, MD 20771. Phone: (301) 614-6164, fax: (301)614-6297, email: gregory.gaspari@saic.com

systems for many years. Efforts to construct covariance functions with vertically variable length fields evolved in response to empirical studies of short-range forecast error statistics by Hollingsworth and Lönnberg (1986) and Lönnberg and Hollingsworth (1986), where it was shown that horizontal forecast error correlation length scales increase significantly with height. The terminology *nonseparable* is used throughout the literature to describe covariance models with length fields that vary with height (Phillips 1986; Bartello and Mitchell 1992; Courtier *et al.* 1998; Rabier *et al.* 1998; Andersson *et al.* 1998; Daley and Barker 2000), since three-dimensional covariance functions with independent horizontal and vertical components are called *separable* (cf. Daley 1991, Sec. 4.3). Short-range forecast errors are known to be smaller over data-dense areas like the northern hemisphere continents than over data-poor areas like the oceans (Bouttier 1994; Courtier *et al.* 1998, Sec. 3(vi); Andersson *et al.* 1998). The covariance functions described below could be applied, for example, with short correlation lengths over data-dense areas and long correlation lengths over the oceans.

Forecast and observation error covariance models in 3D-Var systems are fixed (flow independent) over the entire assimilation, and subject to one or more simplifying assumptions such as homogeneity, isotropy, compact support, and separability (Parrish and Derber 1992; Cohn *et al.* 1998; Courtier *et al.* 1998; Gaspari and Cohn 1999; Daley and Barker 2000). These limitations are also present in 4D-Var systems, since the initial covariance at each analysis cycle is specified as in 3D-Var (Rabier *et al.* 2000; Mahfouf *et al.* 2000; Klinker *et al.* 2000). The new covariance functions constructed below directly extend the single-level covariance functions within the 3D-Var like Physical-space Statistical Analysis System (PSAS; Cohn *et al.* 1998). Since the new covariance functions extend models that are widely employed, development efforts needed to incorporate them into other existing 3D-Var and 4D-Var systems should be modest.

Results are presented in two sections. Section 2 develops mathematical results needed for the construction of global, three-dimensional covariance functions directly in physical space, that depend on a length field. The style of presentation mirrors Gaspari and Cohn (1999, henceforth referred to as GC), with extensive use of results from that article. A first reading of GC is highly recommended as background motivating the results in Sec. 2. Although the theory and constructive techniques presented in GC are general, the results in GC are slanted toward single-level, univariate applications of covariance modeling. In accordance with terminology adopted in GC, and to qualify the extension of single-level univariate covariance functions to multiple levels, the nonseparable covariance functions constructed in this article will be referred to as multi-level. Multi-level covariance functions were introduced in GC, Secs. 3(c) and 4, where multi-level extensions of single-level covariance functions are described using graphs and analytic formulas valid for special cases. This article both extends and complements GC, with greater emphasis given below on relations between the three-dimensional Fourier spectrum and the covariance functions in physical space. A new, first order autoregressive covariance (FOAR) is developed as an example of a continuous, nondifferentiable multi-level covariance. The third-order autoregressive covariance (TOAR) obtained by self-convolution in GC Sec. 4(b) is rederived using Fourier inversion, yielding formulas that more clearly show the relation between the multi-level TOAR and FOAR covariances. The multi-level piecewise rational covariance developed in GC Sec. 4(c) is discussed, with closed form expressions for the most general form of this covariance given in the Appendix. Schur products of single- and multi-level covariances are applied to yield additional multi-level covariances. Combining the multi-level covariance functions constructed below with single-level covariance function examples constructed in GC yields many additional multi-level covariance functions. Multi-level powerlaw covariance functions are also constructed. The powerlaw covariances

have continuous derivatives of all orders, and thus are well-suited for applications requiring broad correlation functions. In the past several years, different forms of the multi-level powerlaw covariance have been applied to model both forecast and observation error covariances within the PSAS. Section 3 describes the powerlaw covariance applied in the PSAS to produce tropically confined and longitudinally symmetric wind increments from spatially sparse wind observations in the tropical lower stratosphere. This new covariance model, which also has a large troposphere to stratosphere gradient in wind length scale, has been successfully applied to physically force a Quasi-Biennial Oscillation (QBO) from wind analysis increments in the Goddard Earth Observing System, Version 4 (GEOS-4), the operational data assimilation system developed at NASA/GSFC. This will be called the baseline GEOS-4 system in what follows. Section 3 below discusses the QBO, describes the new PSAS covariance model developed to force it from sparse wind observations, and also shows a significantly improved QBO representation when compared to the QBO obtained using the baseline GEOS-4 system.

2 Construction of multi-level covariance functions: theory and examples

First we introduce two definitions that provide equivalent tests to determine covariance functions on any set W. Definition 2.1 below extends GC Definition 2.1 to the case of vector-valued random fields.

Definition 2.1 *The multi-level covariance function of a random vector field*

$$\mathbf{X}(\mathbf{r}) := [\, X_1(\mathbf{r}), X_2(\mathbf{r}), \ldots, X_m(\mathbf{r}) \,]^T, \quad \mathbf{r} \in W,$$

is the $m \times m$ matrix function

$$\mathbf{\Gamma}(\mathbf{r}, \mathbf{s}) := < \mathbf{Y}(\mathbf{r})\, \mathbf{Y}(\mathbf{s})^T >, \qquad \mathbf{r}, \mathbf{s} \in W, \tag{1}$$

where

$$\mathbf{Y}(\mathbf{r}) := [\, Y_1(\mathbf{r}), Y_2(\mathbf{r}), \ldots, Y_m(\mathbf{r}) \,]^T, \quad Y_k(\mathbf{r}) := X_k(\mathbf{r}) - < X_k(\mathbf{r}) >, \tag{2}$$

where $X_k(\mathbf{r})$, $k = 1, 2, \ldots, m$, *are real-valued random fields on* W, *and where* $< \cdot >$ *denotes mathematical expectation.* □

For continuous covariance functions, Definition 2.1 is equivalent to the test described below in Definition 2.2 that is based on grid evaluations (cf. Loève 1963, pp. 466-467).

Definition 2.2 *The* $m \times m$ *matrix of functions*

$$\{B_{kl}(\mathbf{r}, \mathbf{s})\}, \qquad \mathbf{r}, \mathbf{s} \in W, \quad k, l = 1, 2, \ldots, m, \tag{3}$$

is a multi-level covariance function on W *if for each positive integer* n, *and for each choice of points* $\mathbf{r}_1, \mathbf{r}_2, \ldots, \mathbf{r}_n$ *in* W, *the* $mn \times mn$ *matrix*

$$\{B_{kl}(\mathbf{r}_i, \mathbf{r}_j)\}, \qquad i, j = 1, 2, \ldots, n, \quad k, l = 1, 2, \ldots, m, \tag{4}$$

is positive semidefinite. □

The following three integration formulas are needed for the construction of multi-level covariance functions given below.

Lemma 2.3 *The Fourier transform (on three-dimensional Euclidean space* R^3*) of* $f(\mathbf{r}) := f_0(\|\mathbf{r}\|)$, *where* $f_0(r) = \exp(-|r|/L)/|r|$, *is given by*

$$\hat{f}(\mathbf{w}) := \int \exp(-i\, \mathbf{w}^T \mathbf{r})\, \frac{\exp(-\|\mathbf{r}\|/L)}{\|\mathbf{r}\|} d\mathbf{r} = \frac{4\pi L^2}{1 + L^2 \|\mathbf{w}\|^2}. \tag{5}$$

Proof: Applying the Hankel transform (cf. GC Eq. (2.31)) yields

$$\hat{f}_0(\|\mathbf{w}\|) = \frac{4\pi}{\|\mathbf{w}\|} \int_0^\infty x f_0(x)\, \sin(\|\mathbf{w}\| x)\, dx = \frac{4\pi L^2}{1 + L^2 \|\mathbf{w}\|^2}. \tag{6}$$

□

Lemma 2.4 *The Fourier transform (on R^3) of $B_1(\mathbf{r}) = \exp(-\|\mathbf{r}\|/L)$ is given by*

$$\hat{B}_1(\mathbf{w}) = \frac{8\pi L^3}{\left(1 + L^2\|\mathbf{w}\|^2\right)^2}. \tag{7}$$

Proof: Apply GC Eq. (2.32):

$$\hat{B}_1(\mathbf{w}) = -\frac{2\pi}{\|\mathbf{w}\|}\frac{d}{d\|\mathbf{w}\|}\hat{B}_0(\|\mathbf{w}\|),$$

where $\hat{B}_0(w) = 2L(1 + w^2L^2)^{-1}$ is given by GC Eq. (4.3). Alternatively, use Folland (1992, p. 247, problem 2). □

Lemma 2.5 *For $\alpha > 0, a > 0, b > 0$,*

$$\begin{aligned} I(a,b,\alpha) &:= \int_{-\infty}^{\infty} \frac{x\,\sin(\alpha x)\,dx}{(x^2+a^2)\,(x^2+b^2)} = \frac{\pi}{a^2-b^2}\left(\exp(-\alpha b) - \exp(-\alpha a)\right), \quad a \neq b, \\ I(a,a,\alpha) &:= \int_{-\infty}^{\infty} \frac{x\,\sin(\alpha x)\,dx}{(x^2+a^2)^2} = \frac{\pi\alpha}{2a}\exp(-\alpha a). \end{aligned} \tag{8}$$

Proof: Both integrals can be evaluated by direct application of the residue theorem (cf. Churchill 1984, Sec. 60). Alternatively, to find $I(a,b,\alpha)$ for $a \neq b$, differentiate both sides of the identity (cf. Churchill 1984, p. 175, problem 4)

$$\int_{-\infty}^{\infty} \frac{\cos(\alpha x)}{(x^2+a^2)\,(x^2+b^2)}\,dx = \frac{\pi}{a^2-b^2}\left(\frac{\exp(-\alpha b)}{b} - \frac{\exp(-\alpha a)}{a}\right) \tag{9}$$

with respect to α. The expression for $I(a,a,\alpha)$ can be found by taking the limit of both sides of $I(a,b,\alpha)$ as b tends to a. □

Example 2.6 below extends the so-called *powerlaw* of GC Sec. 4(d). These functions are everywhere infinitely differentiable and thus are useful in applications where smoothness is required. In Section 3 below, a multi-level powerlaw function with long stratospheric length scales is shown to produce the approximately zonal analysis increments for wind needed as forcing for a zonally symmetric quasi-biennial oscillation (QBO) from observational wind data. Multi-level covariance functions with zero, two, and three derivatives at zero separation are constructed following the multi-level powerlaw example.

Example 2.6 *Given any length scales $L_k > 0$, $k = 1, 2, \ldots, m$, define*

$$P_{kl}(\mathbf{r}, \mathbf{s}) := \frac{L_k L_l}{L_{kl}^{\,2}} \frac{1}{1 + 0.5(\|\mathbf{r} - \mathbf{s}\|/L_{kl})^2}, \quad \mathbf{r}, \mathbf{s} \in R^3, \quad L_{kl} := 0.5(L_k + L_l). \tag{10}$$

The $m \times m$ matrix of functions

$$\{P_{kl}(\mathbf{r}, \mathbf{s})\}, \quad \mathbf{r}, \mathbf{s} \in R^3, \quad k, l = 1, 2, \ldots m, \tag{11}$$

is a multi-level (powerlaw) covariance function.

Proof: To verify Definition 2.2, we must show that

$$\sum_{k,l=1}^{m} \sum_{i,j=1}^{n} P_{kl}(\mathbf{r}_i, \mathbf{r}_j)\, c_{ik} c_{jl} \;\geq\; 0 \tag{12}$$

for arbitrary constants c_{ik}, $i = 1, 2, \ldots, n$, $k = 1, 2, \ldots, m$. Applying Lemma 2.3 with $L = 1$ (interchange the roles of $\mathbf{r}$ and $\mathbf{w}$) yields

$$\int \exp(-i\, \mathbf{w}^T \mathbf{r})\, \frac{\exp(-\|\mathbf{w}\|)}{\|\mathbf{w}\|} d\mathbf{w} \;=\; \frac{4\pi}{1 + \|\mathbf{r}\|^2}. \tag{13}$$

Using Eq. (13) and the change of variable $(L_{kl}\sqrt{2})\, \mathbf{u} = \mathbf{w}$ yields

$$2\pi P_{kl}(\mathbf{r}_i, \mathbf{r}_j) = L_k L_l \int \exp(-i\, \mathbf{u}^T(\mathbf{r}_i - \mathbf{r}_j))\, \frac{\exp(-L_{kl}\sqrt{2}\|\mathbf{u}\|)}{\|\mathbf{u}\|}\, d\mathbf{u}. \tag{14}$$

Using the identity

$$|\mathbf{c}^T \mathbf{z}|^2 \;=\; \sum_{k,l=1}^{m} \sum_{i,j=1}^{n} L_k L_l\, \exp(-\|\mathbf{u}\| L_{kl}\sqrt{2})\, \exp(-i\, \mathbf{u}^T(\mathbf{r}_i - \mathbf{r}_j)) c_{ik} c_{jl}, \tag{15}$$

where the mn-vectors $\mathbf{c}$ and $\mathbf{z}$ are defined by:

$$\begin{aligned} \mathbf{c} \;&:=\; [c_{11}, c_{21}, \ldots, c_{n1}, c_{12}, \ldots, c_{n2}, \ldots, c_{1m}, \ldots, c_{nm}]^T, \\ \mathbf{z} \;&:=\; [z_{11}, z_{21}, \ldots, z_{n1}, z_{12}, \ldots, z_{n2}, \ldots, z_{1m}, \ldots, z_{nm}]^T, \\ z_{jl} \;&:=\; L_l\; \exp(i\mathbf{u}^T \mathbf{r}_j) \exp(-0.5\, \|\mathbf{u}\| L_l \sqrt{2}),\; j = 1, \ldots, n, \quad l = 1, \ldots, m, \end{aligned} \tag{16}$$

in Eq. (14) yields

$$2\pi \sum_{k,l=1}^{m} \sum_{i,j=1}^{n} P_{kl}(\mathbf{r}_i, \mathbf{r}_j)\, c_{ik} c_{jl} \;=\; \int \frac{|\mathbf{c}^T \mathbf{z}|^2}{\|\mathbf{u}\|} d\mathbf{u} \;\geq\; 0. \tag{17}$$

This completes the proof. □

Theorem 2.7 below generalizes GC Theorem 2.10 to a necessary and sufficient condition that characterizes all homogeneous multi-level covariance functions that are integrable over R^N. This result was first proven by Cramér (1940; cf. Yaglom 1987, pp. 314-315). A special case of this result can be applied to prove that the examples constructed below using cross-convolutions over R^3 are multi-level covariances– see the remarks following Thm. 2.7.

Theorem 2.7 *Define*

$$\{B_{kl}(\mathbf{r},\mathbf{s})\}, \qquad \mathbf{r},\mathbf{s} \in R^N, \quad k,l = 1,2,\ldots,m, \tag{18}$$

where each $B_{kl}(\mathbf{r},\mathbf{s})$ is a homogeneous function on R^N, and where each $B_{kl}(\mathbf{r},\mathbf{0})$ is integrable over R^N. Then $\{B_{kl}(\mathbf{r},\mathbf{s})\}$ is a multi-level covariance function if, and only if, the $m \times m$ spectral density matrices

$$\int \{B_{kl}(\mathbf{r},\mathbf{0})\, \exp(-i\,\mathbf{w}^T\mathbf{r})\,\}d\mathbf{r}, \quad k,l = 1,2,\ldots,m, \tag{19}$$

are positive semidefinite for each $\mathbf{w} \in R^N$. □

Remarks: Theorem 2.7 and GC Theorem 2.9 together imply that the $m \times m$ matrix of convolutions over R^N:

$$\{(h_k * h_l)(\mathbf{r}-\mathbf{s})\}, \quad \mathbf{r},\mathbf{s} \in R^N, \quad k,l = 1,2,\ldots,m, \tag{20}$$

is a multi-level covariance function, if each h_k is a real-valued, radially symmetric function in $L^1(R^N) \cap L^2(R^N)$. This follows from the fact that the $m \times m$ spectral density matrix of Eq. (20) is the rank-one outer product

$$\{\hat{h_k}(\mathbf{w})\hat{h_l}(\mathbf{w})\}, \quad k,l = 1,2,\ldots,m, \tag{21}$$

(cf. GC Theorem 2.9) and thus is positive semidefinite for each $\mathbf{w} \in R^N$.

Observe that Thm. 2.7 was not applied in the proof of Example 2.6 above, since the multi-level powerlaw is not integrable over R^3. □

The convolution integrals in Eq. (20) for the case of R^3 were reduced to a simpler form in GC Sec. 3(c). Several worked examples where these convolution integrals are then evaluated in closed form were given in GC Sec. 4. Three examples are provided below to complement and extend results presented in GC Sec. 4. The multi-level FOAR covariance given in Example 2.8 is new. It is non-differentiable at the origin, having cusp-like behavior, and thus is useful for modeling covariances with a slowly decaying spectral density (cf. Ménard *et al.* 2000, Sec. 5). Compactly supported multi-level TOAR-like covariances were constructed in GC Sec. 4(b) through self-convolution of FOAR-like functions over R^3, however, general formulas were not given in the case where the length scales are different. Example 2.9 below provides explicit, simplified expressions for the multi-level TOAR covariance considered in GC Sec. 4(b). Recall that the TOAR covariance has four continuous derivatives at the origin. Multi-level compactly supported 5th-order piecewise rational functions extending GC Sec. 4(c) are given in Example 2.10 below. These functions have two continuous derivatives at the origin.

Example 2.8 *Define*

$$\begin{aligned} F_{kl}(\mathbf{r},\mathbf{s}) &:= \frac{2\sqrt{{L_k}^3 {L_l}^3}}{({L_k}^2 - {L_l}^2)} \left(\frac{\exp(-\|\mathbf{r}-\mathbf{s}\|/L_k) - \exp(-\|\mathbf{r}-\mathbf{s}\|/L_l)}{\|\mathbf{r}-\mathbf{s}\|} \right), \ \mathbf{r} \neq \mathbf{s}, \ L_k \neq L_l, \\ F_{kl}(\mathbf{r},\mathbf{r}) &:= \frac{\sqrt{L_k L_l}}{L_{kl}}, \quad L_{kl} := 0.5(L_k + L_l), \\ F_{kk}(\mathbf{r},\mathbf{s}) &:= \exp(-\|\mathbf{r}-\mathbf{s}\|/L_k), \quad k,l = 1,2,\ldots,m. \end{aligned} \tag{22}$$

The $m \times m$ matrix of functions

$$\{F_{kl}(\mathbf{r},\mathbf{s})\}, \quad \mathbf{r},\mathbf{s} \in R^3, \quad k,l = 1,2,\ldots m, \tag{23}$$

is a multi-level (FOAR) covariance function.

Proof: To apply Thm. 2.7, it is shown that the multi-level FOAR function is a matrix of cross-convolutions over R^3. To this end, define

$$f_k(\mathbf{r}) := \frac{\exp(-\|\mathbf{r}\|/L_k)}{\|\mathbf{r}\|\sqrt{2\pi L_k}}, \quad k = 1, 2, \ldots, m, \tag{24}$$

and apply Lemma 2.3 to obtain

$$\hat{f}_k(\mathbf{w}) = \frac{\sqrt{8\pi {L_k}^3}}{1 + {L_k}^2 \|\mathbf{w}\|^2}. \tag{25}$$

Lemma 2.4 shows that the Fourier transform of $F_{kk}(\mathbf{r}, \mathbf{0})$ is the square of $\hat{f}_k(\mathbf{w})$:

$$\int F_{kk}(\mathbf{r}, \mathbf{0}) \, \exp(-i \, \mathbf{w}^T \mathbf{r}) \, d\mathbf{r} = \frac{8\pi {L_k}^3}{\left(1 + {L_k}^2 \|\mathbf{w}\|^2\right)^2}, \tag{26}$$

so that $F_{kk}(\mathbf{r}, \mathbf{s}) = (f_k * f_k)(\mathbf{r} - \mathbf{s})$. To complete the proof, it is shown that $F_{kl}(\mathbf{r}, \mathbf{s})$ is the inverse Fourier transform over R^3 of $\hat{f}_k(\mathbf{w}) \, \hat{f}_l(\mathbf{w})$, i.e.,

$$F_{kl}(\mathbf{r}, \mathbf{s}) = (f_k * f_l)(\mathbf{r} - \mathbf{s}) = \frac{1}{8\pi^3} \int \hat{f}_k(\mathbf{w}) \, \hat{f}_l(\mathbf{w}) \, \exp(i \mathbf{w}^T (\mathbf{r} - \mathbf{s})) \, d\mathbf{w}. \tag{27}$$

Let I_1 be the value of the integral in Eq. (27), and let $a_k := 1/L_k$, $a_l := 1/L_l$, where $a_k \neq a_l$. Applying the Hankel transform yields

$$\begin{aligned} I_1 &= \frac{2}{\pi \|\mathbf{r} - \mathbf{s}\| \sqrt{L_k L_l}} \int_{-\infty}^{\infty} \frac{x \sin(\|\mathbf{r} - \mathbf{s}\| x)}{(x^2 + a_l{}^2)(x^2 + a_k{}^2)} \, dx \\ &= \frac{2}{\pi \|\mathbf{r} - \mathbf{s}\| \sqrt{L_k L_l}} \, I(a_l, a_k, \|\mathbf{r} - \mathbf{s}\|) \\ &= \frac{2}{\|\mathbf{r} - \mathbf{s}\| \sqrt{L_k L_l}} \left(\frac{\exp(-\|\mathbf{r} - \mathbf{s}\| a_k) - \exp(-\|\mathbf{r} - \mathbf{s}\| a_l)}{a_l{}^2 - a_k{}^2} \right) \\ &= F_{kl}(\mathbf{r}, \mathbf{s}), \end{aligned} \tag{28}$$

where Lemma 2.5 was applied to evaluate the integral. □

Example 2.9 *Define*

$$\begin{aligned} T_{kl}(\mathbf{r}, \mathbf{s}) &:= \frac{8\sqrt{{L_k}^3 {L_l}^3}}{\left({L_k}^2 - {L_l}^2\right)^2} \left(L_k F_{kk}(\mathbf{r}, \mathbf{s}) + L_l F_{ll}(\mathbf{r}, \mathbf{s}) - 2\sqrt{L_k L_l} F_{kl}(\mathbf{r}, \mathbf{s}) \right), \quad L_k \neq L_l, \\ T_{kk}(\mathbf{r}, \mathbf{s}) &:= \left(1 + \frac{\|\mathbf{r} - \mathbf{s}\|}{L_k} + \frac{\|\mathbf{r} - \mathbf{s}\|^2}{3{L_k}^2} \right) F_{kk}(\mathbf{r}, \mathbf{s}), \quad k = 1, 2, \ldots, m. \end{aligned} \tag{29}$$

The $m \times m$ matrix of functions

$$\{T_{kl}(\mathbf{r},\mathbf{s})\}, \quad \mathbf{r},\mathbf{s} \in R^3, \quad k,l = 1,2,\ldots m, \tag{30}$$

is a multi-level (TOAR) covariance function.

Proof: To apply Thm. 2.7, it is shown that the multi-level TOAR function is a matrix of cross-convolutions over R^3. To this end, define

$$g_k(\mathbf{r}) := \frac{\exp(-\|\mathbf{r}\|/L_k)}{\sqrt{\pi {L_k}^3}}, \quad k = 1,2,\ldots,m, \tag{31}$$

and apply Lemma 2.4 to obtain

$$\hat{g}_k(\mathbf{w}) = \frac{8\sqrt{\pi {L_k}^3}}{\left(1 + {L_k}^2\|\mathbf{w}\|^2\right)^2}. \tag{32}$$

First it is shown that

$$\hat{T}_{kk}(\mathbf{w}) = \hat{g}_k(\mathbf{w})^2 = \frac{64\pi {L_k}^3}{\left(1 + {L_k}^2\|\mathbf{w}\|^2\right)^4} = \frac{64\pi {a_k}^5}{\left({a_k}^2 + \|\mathbf{w}\|^2\right)^4}, \tag{33}$$

where $a_k := 1/L_k$, implying that $T_{kk}(\mathbf{r},\mathbf{s}) = (g_k * g_k)(\mathbf{r}-\mathbf{s})$. Applying the Hankel transform yields

$$\begin{aligned}
(g_k * g_k)(\mathbf{r}-\mathbf{s}) &= \frac{1}{8\pi^3}\int \hat{g}_k(\mathbf{w})^2 \exp(i\mathbf{w}^T(\mathbf{r}-\mathbf{s}))\, d\mathbf{w} \\
&= \frac{16{a_k}^5}{\pi\|\mathbf{r}-\mathbf{s}\|}\int_{-\infty}^{\infty} \frac{x\sin(\|\mathbf{r}-\mathbf{s}\|x)}{(x^2+{a_k}^2)^4}\, dx \\
&= \frac{8{a_k}^5}{3\pi}\int_{-\infty}^{\infty} \frac{\cos(\|\mathbf{r}-\mathbf{s}\|x)}{(x^2+{a_k}^2)^3}\, dx,
\end{aligned} \tag{34}$$

where the third equality in Eq. (34) was obtained using integration by parts. To simplify Eq. (34), recall the relation between the one-dimensional SOAR function and its spectral density function (cf. Daley 1991; Churchill 1984, p. 176, problem 6):

$$I_2(a_k,\|\mathbf{r}\|) := \int_{-\infty}^{\infty} \frac{\cos(\|\mathbf{r}\|x)}{(x^2+{a_k}^2)^2}\, dx = \frac{\pi}{2{a_k}^3}\Big(1 + a_k\|\mathbf{r}\|\Big)\exp\Big(-a_k\|\mathbf{r}\|\Big). \tag{35}$$

Differentiating both sides of Eq. (35) with respect to a_k and substituting into Eq. (34) yields

$$(g_k * g_k)(\mathbf{r}-\mathbf{s}) = -\frac{2{a_k}^4}{3\pi} I_2{}'(a_k, \|\mathbf{r}-\mathbf{s}\|) = T_{kk}(\mathbf{r},\mathbf{s}). \tag{36}$$

Now let $a_l := 1/L_l$, with $a_k \neq a_l$. To complete the proof, it is shown that

$$\begin{aligned} \hat{T}_{kl}(\mathbf{w}) = \hat{g}_k(\mathbf{w})\hat{g}_l(\mathbf{w}) &= \frac{64\pi\sqrt{{L_k}^3{L_l}^3}}{\left(1+{L_k}^2\|\mathbf{w}\|^2\right)^2\left(1+{L_l}^2\|\mathbf{w}\|^2\right)^2} \\ &= \frac{64\pi\sqrt{{a_k}^5{a_l}^5}}{\left({a_k}^2+\|\mathbf{w}\|^2\right)^2\left({a_l}^2+\|\mathbf{w}\|^2\right)^2}. \end{aligned} \tag{37}$$

Applying the Hankel transform yields

$$\begin{aligned} (g_k * g_l)(\mathbf{r}-\mathbf{s}) &= \frac{1}{8\pi^3}\int \hat{g}_k(\mathbf{w})\hat{g}_l(\mathbf{w})\,\exp(i\mathbf{w}^T(\mathbf{r}-\mathbf{s}))\,d\mathbf{w} \\ &= \frac{16\sqrt{{a_k}^5{a_l}^5}}{\pi\|\mathbf{r}-\mathbf{s}\|}\int_{-\infty}^{\infty}\frac{x\sin(\|\mathbf{r}-\mathbf{s}\|x)}{(x^2+{a_k}^2)^2(x^2+{a_l}^2)^2}\,dx \\ &= \frac{16\sqrt{{a_k}^5{a_l}^5}}{\pi\|\mathbf{r}-\mathbf{s}\|({a_k}^2-{a_l}^2)^2}\Big(I(a_k,a_k)+I(a_l,a_l)-2I(a_k,a_l)\Big), \end{aligned} \tag{38}$$

where the third equality is obtained by expanding $(x^2+{a_k}^2)^{-1}(x^2+{a_l}^2)^{-1}$ into partial fractions, squaring the result, and applying Lemma 2.5, where $I(a,b) := I(a,b,\|\mathbf{r}-\mathbf{s}\|)$ is abbreviated. Substituting

$$\sqrt{L_kL_l}\,F_{kl}(\mathbf{r},\mathbf{s}) = \frac{2}{\pi\|\mathbf{r}-\mathbf{s}\|}\,I(a_k,a_l,\|\mathbf{r}-\mathbf{s}\|) \tag{39}$$

into Eq. (38) and simplifying yields the result. □

Example 2.10 Given scalars a_k and c, define

$$h_k(\mathbf{r}) := \begin{cases} (2(a_k-1)\|\mathbf{r}\|/c+1)n_k & 0\le\|\mathbf{r}\|\le c/2 \\ 2a_k(1-\|\mathbf{r}\|/c)n_k & c/2\le\|\mathbf{r}\|\le c \\ 0 & c\le\|\mathbf{r}\| \end{cases}, \quad k=1,2,\ldots,m, \tag{40}$$

where $n_k := (2+44a_k^2+6a_k)^{-1/2}$. Closed form expressions for the convolution integrals $h_k * h_l$ over R^3

$$(h_k * h_l)(\mathbf{r}-\mathbf{s}) = \begin{cases} f_1(\|\mathbf{r}-\mathbf{s}\|/c)n_kn_l, & 0\le\|\mathbf{r}-\mathbf{s}\|\le c/2 \\ f_2(\|\mathbf{r}-\mathbf{s}\|/c)n_kn_l, & c/2\le\|\mathbf{r}-\mathbf{s}\|\le c \\ f_3(\|\mathbf{r}-\mathbf{s}\|/c)n_kn_l, & c\le\|\mathbf{r}-\mathbf{s}\|\le 3c/2 \\ f_4(\|\mathbf{r}-\mathbf{s}\|/c)n_kn_l, & 3c/2\le\|\mathbf{r}-\mathbf{s}\|\le 2c \\ 0 & 2c\le\|\mathbf{r}-\mathbf{s}\| \end{cases}, \tag{41}$$

are given in the Appendix. The case $a_k = a_l$ is illustrated in GC Figs. 7,8. If $a_k = a_l = 1/2$ then Eq. (41) reduces to GC Eq. (4.10). □

Theorem 2.11 below provides an important practical technique for the construction of multi-level covariance functions using the Schur product.

Theorem 2.11 *If $C(\mathbf{r}, \mathbf{s})$ is a covariance function on a set W and*

$$\{B_{kl}(\mathbf{r}, \mathbf{s})\}, \qquad \mathbf{r}, \mathbf{s} \in W, \quad k, l = 1, 2, \ldots, m, \tag{42}$$

is a multi-level covariance function on W, then

$$\{C(\mathbf{r}, \mathbf{s})\, B_{kl}(\mathbf{r}, \mathbf{s})\}, \qquad \mathbf{r}, \mathbf{s} \in W, \quad k, l = 1, 2, \ldots, m, \tag{43}$$

is a multi-level covariance function on W.

Proof: Since $C(\mathbf{r}, \mathbf{s})$ is a covariance function on W, the $mn \times mn$ matrix

$$\{C_{kl}(\mathbf{r}, \mathbf{s})\}, \; C_{kl} := C, \quad \mathbf{r}, \mathbf{s} \in W, \quad k, l = 1, 2, \ldots, m, \tag{44}$$

is a multi-level covariance function on W:

$$\begin{aligned} \sum_{k,l=1}^{m} \sum_{i,j=1}^{n} C(\mathbf{r}_i, \mathbf{r}_j) b_{ik} b_{jl} &= \sum_{i,j=1}^{n} C(\mathbf{r}_i, \mathbf{r}_j) \sum_{k,l=1}^{m} b_{ik} b_{jl} \\ &= \sum_{i,j=1}^{n} C(\mathbf{r}_i, \mathbf{r}_j) \sum_{k=1}^{m} b_{ik} \sum_{l=1}^{m} b_{jl} \\ &= \sum_{i,j=1}^{n} C(\mathbf{r}_i, \mathbf{r}_j)\, \beta_i \beta_j \geq 0, \qquad \beta_i := \sum_{k=1}^{m} b_{ik}. \end{aligned} \tag{45}$$

The theorem follows by applying the Schur product theorem to the two positive semidefinite $mn \times mn$ matrices $\{C_{kl}(\mathbf{r}_i, \mathbf{r}_j)\}$ and $\{B_{kl}(\mathbf{r}_i, \mathbf{r}_j)\}$. □

Example 2.6 and Theorem 2.11 above provide tools needed to construct nonseparable extensions using Schur products. One such extension, summarized in Example 2.12 below, has been applied in the Physical-space Statistical Analysis System (PSAS) (Cohn *et al.* 1998) for the past several years.

Example 2.12 *The $m \times m$ matrix of functions*

$$P_{kl}(\mathbf{r},\mathbf{s})\, C(\mathbf{r},\mathbf{s}), \quad \mathbf{r},\mathbf{s} \in R^3, \quad k,l = 1,2,\ldots,m, \tag{46}$$

where $P_{kl}(\mathbf{r},\mathbf{s})$ is the powerlaw defined in Example 2.6 above, and where $C(\mathbf{r},\mathbf{s})$ is any correlation function on R^3, is a multi-level covariance function.

Remark: The PSAS application of Example 2.12 in the baseline GEOS-4 system uses C represented by GC, Eq. (4.10). □

Theorem 2.13 below generalizes GC Theorem 2.11 to a necessary and sufficient condition that characterizes all continuous isotropic multi-level covariance functions on the $(N-1)$-dimensional sphere S^{N-1}. This result was first proven by Hannan (1970; cf. Yaglom p. 387).

Theorem 2.13 *Consider the $m \times m$ matrix of functions*

$$\{B_{kl}(\mathbf{r},\mathbf{s})\}, \qquad \mathbf{r},\mathbf{s} \in S^{N-1}, \quad k,l = 1,2,\ldots,m, \tag{47}$$

where each $B_{kl}(\mathbf{r},\mathbf{s})$ is a continuous isotropic function on S^{N-1}. Then $\{B_{kl}(\mathbf{r},\mathbf{s})\}$ is a multi-level covariance function if, and only if,

$$\{B_{kl}(\mathbf{r},\mathbf{s})\} = \sum_{i=0}^{\infty} \mathbf{A}_i C_i^{(N-2)/2}(\mathbf{r}^T\mathbf{s}), \tag{48}$$

where each $\mathbf{A}_i$ is a positive semidefinite $m \times m$ matrix, and where $C_i^{(N-2)/2}$ are Gegenbauer polynomials of degree m and order $(N-2)/2$. □

Remark: Isotropic multi-level covariance functions on S^{N-1} are readily obtained using the above results developed for R^N simply by restricting the points from R^N to S^{N-1}. This point is further elaborated in GC Sec. 2(c). □

3 An application: tropical stratospheric winds

The QBO dominates the dynamics of the equatorial stratosphere between about 70 hPa and 10 hPa, with downward propagating, zonally symmetric easterly and westerly wind regimes. Observations of the QBO indicate that it is symmetric about the Equator with a maximum amplitude of about 20 ms^{-1} and has an approximate Gaussian half-width of about 12° in latitude (cf. Holton 1992, pp. 424–425). Dynamical aspects of the QBO are generally illustrated using a time-height cross section of monthly-mean equatorial zonal wind (e.g. Baldwin *et al.* 2001). It is commonly accepted that the QBO is approximately zonally symmetric (Belmont and Dartt 1968), although a recent study by Hamilton *et al.* (2004) showed that zonal asymmetries can be found at 10 hPa during the westerly phase of the QBO. This point will be further elaborated below.

Efforts to understand the QBO using observational data are complicated by the lack of available in-situ wind observations in the near-equatorial stratosphere above 50 hPa. Radiosonde reports are scarce, since many balloons burst near the very cold tropical tropopause (Hamilton *et al.* 2004). As a result, there have been difficulties in generating accurate QBO signals in some assimilated datasets (cf. Randel *et al.* 2004). A common problem is that the amplitude of the QBO is often underestimated in comparison with radiosonde measurements (Pawson and Fiorino, 1998) although the ECMWF Reanalysis-40 (ERA-40) does very well (cf. Randel *et al.* 2004).

Figure 1 illustrates that radiosonde observations available to reproduce a QBO are concentrated in the Far East. The top panel of Fig. 1 shows the station averaged value of the 10 hPa zonal wind, at 00 GMT and rounded to the nearest integer, for each station reporting 5 or more times in November 1991. The influence these observations have on the assimilated zonal wind is discussed below. The middle panel shows the number of reports corresponding to each location shown in the top panel. For instance, the average wind

speed of 7 ms^{-1} in the top panel at the Singapore radiosonde (1.37° N, 103.98° E) is over 26 of 30 possible 00 GMT reports. The bottom panel shows the number of radiosonde stations reporting 5 or more times at 50 hPa. A typical distribution of radiosonde reports on mandatory pressure levels between 10 hPa and 50 hPa is less dense than the lower panel, and more dense than in the middle panel. Dynamical properties of the QBO are often illustrated using time series of the zonal wind observed at the Singapore radiosonde, due to the sparsity of available observations, and since the reports from this station are both consistent and of high quality. A centered 10-day moving average of zonal wind observations from 10 hPa to 50 hPa at Singapore is shown in Fig. 2 from May 1991 through November 1995. Several observed properties of the QBO are clear in this figure. For example, easterly and westerly wind regimes alternate, the maximum amplitude is approximately 20 ms^{-1} from 10 hPa to 30 hPa, and the downward propagation of zonal wind occurs without loss of amplitude from 10 hPa to 30 hPa.

To generate a QBO in GEOS-4, tropically confined and longitudinally elongated zonal wind analysis increments are needed to effect the rapid QBO phase transitions illustrated in Fig. 2. Two multi-level covariance models were tested in GEOS-4. The model used to improve the QBO representation, henceforth known as model A, is a powerlaw in the form of Example 2.6 with tropically confined and longitudinally elongated wind correlation length scales. Model B is the so-called ***windowed powerlaw*** used in the baseline GEOS-4 data assimilation system, in the form given in Example 2.12. A static PSAS analysis using a single Singapore radiosonde sounding at 1200 GMT on 21 September 1999 is described below for the purpose of illustrating key differences between models A and B. Figure 3 shows the correlation length scale differences between models A and B (left panel) and the observed-minus-forecast (OMF) residuals used in this static PSAS analysis (right panel). The length scales are identical for $p \geq 200$ hPa.

Model A has much larger length scales than model B for $p < 200$ hPa. The PSAS zonal wind analysis increments produced using models A and B are shown in Figs. 4 and 5. At 2° N (Fig. 4), the increments are similar where the length scale profiles shown in Fig. 3 are identical, but their longitudinal structure reflects the stratospheric length scale differences. The analysis increments near Singapore are, as expected, a fraction of the nearby OMF values (Fig. 3). Such increments illustrate a typical action of the gain matrix on the OMF vector (cf. Daley 1991, p. 377). Figure 5 shows horizontal maps at 10 hPa of the increments seen in Fig. 4, illustrating the approximate longitudinal symmetry of the analysis increments produced using model A, and the more confined meridional scale.

Assimilation experiments A and B, using GEOS-4 with covariance models A and B, respectively, were configured to study the impacts on the assimilated QBO of using the elongated correlation length fields in the tropical stratosphere. The analysis focuses on the representation of the winds and shear zones at the onset of the westerly wind regime at 10 hPa, between November 1991 and January 1992. The two experiments were initialized with identical states on 1 May 1991. To ensure that both experiments used the same tropical wind observations, the GEOS-4 quality control settings were updated to accept all radiosondes in the tropical lower stratosphere.

The first major differences between the two experiments occur at the onset of the 10 hPa phase transition in late October 1991 (see Fig. 2). Figure 6 shows aspects of the zonal wind at 00 GMT on 30 November 1991, approximately one month following the onset of westerly winds at Singapore. The upper two panels illustrate typical differences between the vertical structure of the zonal-mean zonal winds in the two assimilation experiments. Experiment A represents a plausible zonal-mean wind field with greater sensitivity to the observed vertical shear (Fig. 2) than Experiment B. The strong easterlies in Experiment B resemble typical observations seen several months prior to the QBO

phase transition. The difference between the two zonal averages reveals the substantial positive impact obtained by stretching the wind correlation length field in longitude. The shear zones in Experiment A seen near 10 hPa and 60 hPa reflect the wind shear present in the observations on 30 November 1991. The large differences near 10 hPa illustrate a systematic difference between the two experiments during the entire QBO phase change, while the differences near 60 hPa are primarily due to less systematic variations in the radiosonde observations. The profiles shown in the lower right panel of Fig. 6 illustrate differences between the local analysis near Singapore and the zonally averaged zonal-mean wind field in both experiments. In Experiment A, there is close agreement between the local analysis near Singapore and the zonal average on the latitude circle. The corresponding profiles for Experiment B are less similar due to the short correlation length scales. Lack of sufficient "spreading" of the analysis increments in Experiment B causes the wind shear near 10 hPa to be misrepresented. Figure 7 shows the 10 hPa winds and their analysis increments for Experiments A and B, averaged over the 00 GMT data for November 1991. This figure clearly shows the introduction of westerly winds near the Equator in Experiment A, and the remains of a strong easterly flow in Experiment B. There is some zonal asymmetry in Experiment A, with two wind maxima of 12 ms^{-1} over the Southern Indian Ocean and 9 ms^{-1} over the eastern Pacific, with weak easterlies over the Atlantic. The analysis increments shown in the lower panels can be viewed as typical corrections applied every 12 hours (when radiosondes are present) to the background zonal wind. The analysis increments in Experiment A are small and quite symmetric near the equator. The small size of the increments (fractions of one meter per second) indicates the model and observations are working in harmony. Imposing the zonally elongated analysis increments means that initial changes are spread over a wider longitude range, allowing the model to sustain a slowly increasing region of

westerlies. This is not the case in Experiment B, where the localized analysis increments apparently have no lasting effect on the zonally averaged zonal wind field. Since these analysis increments are both localized and intermittent (every 12 hours), advection of the strong easterlies quickly leads to their local replenishment, so that a large difference between model forecast and observations remains and the model is not able to develop the observed westerly winds. By January 1992, the transition to westerlies in Experiment A has occurred at all longitudes (Fig. 8), with a displacement of the westerly maxima to the North of the Equator. In experiment B, the wind remains easterly and the analysis increments retain a complex structure.

4 Concluding Remarks

Theoretical and practical mathematical results were developed to construct covariance functions dependent on variable length fields. These general results could potentially be applied in many application areas requiring parametrized covariance models having a modest degree of additional flexibility beyond homogeneous and isotropic models. The specific application to improve the QBO illustrates the ability of the covariance model to incorporate both tropospheric and stratospheric length scales appropriate to different regions of the atmosphere. Other applications will be explored in future work.

5 Appendix

The functions $f_1, \ldots, f_4$ defined in Eq. (41) are given by:

$$f_1(z) = b_{15}z^5 + b_{14}z^4 + b_{13}z^3 + b_{12}z^2 + b_{10}, \tag{49}$$

$$f_2(z) = b_{25}z^5 + b_{24}z^4 + b_{23}z^3 + b_{22}z^2 + b_{21}z + b_{20} + d_{21}z^{-1},$$

$$
\begin{aligned}
f_3(z) &= b_{35}z^5 + b_{34}z^4 + b_{33}z^3 + b_{32}z^2 + b_{31}z + b_{30} + d_{31}z^{-1}, \\
f_4(z) &= \frac{8a_ka_l}{3}\left(2z^5 - 12z^4 + 15z^3 + 40z^2 - 120z + 96 - 16z^{-1}\right), \\
b_{15} &:= 16(-3 - 7a_ka_l + 4a_k + 4a_l)/3, \\
b_{14} &:= 16(1 + 2a_ka_l - a_k - a_l), \\
b_{13} &:= 10(1 + 8a_ka_l - 2a_k - 2a_l), \\
b_{12} &:= -40(1 + 8a_ka_l - a_k - a_l)/3, \\
b_{10} &:= 2 + 44a_ka_l + 3a_k + 3a_l, \\
b_{25} &:= 16(1 + 5a_ka_l - 3a_k - 3a_l)/3, \\
b_{24} &:= 8(-2 - 8a_ka_l + 5a_k + 5a_l), \\
b_{23} &:= 10, \\
b_{22} &:= 20(2 + 20a_ka_l - 11a_k - 11a_l)/3, \\
b_{21} &:= 5(-4 - 36a_ka_l + 13a_k + 13a_l), \\
b_{20} &:= (16 + 204a_ka_l - 35a_k - 35a_l)/2, \\
d_{21} &:= (-8 - 84a_ka_l + 29a_k + 29a_l)/12, \\
b_{35} &:= 16(-3a_ka_l + a_k + a_l)/3, \\
b_{34} &:= 8(8a_ka_l - 3a_k - 3a_l), \\
b_{33} &:= -20(2a_ka_l - a_k - a_l), \\
b_{32} &:= -20(20a_ka_l - 9a_k - 9a_l)/3, \\
b_{31} &:= 5(44a_ka_l - 27a_k - 27a_l), \\
b_{30} &:= -(244a_ka_l - 189a_k - 189a_l)/2, \\
d_{31} &:= (460a_ka_l - 243a_k - 243a_l)/12.
\end{aligned}
\tag{50}
$$

ACKNOWLEDGMENTS

S. Pawson's work was supported in part by NASA Award NAG5-12162 "Reanalysis for Studies of Trace gases in the Stratosphere".

REFERENCES

Andersson, E., Haseler, J, Undén, P., Courtier, P., Kelly, G, Vasiljević, D., Branković, C, Cardinali, C., Gaffard, C., Hollingsworth, A., Jakob, C, Janssen, P., Klinker, E., Laanzinger, A., Miller, M., Rabier, F., Simmons, A., Strauss, B., Thépaut, J.-N. and Viterbo, P. 1998 The ECMWF implementation of three dimensional variational assimilation (3D-Var). Part III: Experimental results. *Q. J. R. Meteorol. Soc.*, **124**, 1831–1860

Baldwin, M. P., Gray, L. J., Dunkerton, T. J., Hamilton, K, Haynes, P. H., Randel, W. J., Holton, J. R., Alexander, M. J., Hirota, I., Horinouchi, T., Jones, D. B. A., Kinnersley, J. S., Marquardt, C., Sato, K, and Takahashi, M. 2001 The Quasi-Biennial Oscillation. *Reviews of Geophysics*, **39,2**, 179–229

Bartello, P. and Mitchell, H. L. 1992 A continuous three-dimensional model of short-range forecast error covariances. *Tellus*, **44A**, 217–235

Belmont, A. D. and Dartt, D. G. 1968 Variation with longitude of the quasi-biennial oscillation. *Mon. Weather Rev.*, **96**, 767–777

Bouttier, F. 1994 A dynamical estimation of forecast error covariances in an assimilation system. *Mon. Weather Rev.*, **122**, 2376–2390

Churchill, R. V. and Brown, J. W. 1984 *Complex variables and applications, 4th ed.* McGraw-Hill, New York

Cohn, S. E., da Silva, A., Guo, J., Sienkiewicz, M., and Lamich, D. 1998 Assessing the effects of data selection with the DAO Physical-space Statistical Analysis System. *Mon. Weather Rev.*, **126**, 2913–2926

Courtier, P., Andersson, E., Heckley, W., Pailleux, J., Vasiljević, D., Hamrud, M., Hollingsworth, A., Rabier, F., and Fisher, M. 1998 The ECMWF implementation of three dimensional variational assimilation (3D-Var). Part I: Formulation. *Q. J. R. Meteorol. Soc.*, **124**, 1783–1808

Cramer, H. 1940 On the theory of stationary random processes. *Ann. Math.*, **41**, 215–230

Daley, R. 1991 *Atmospheric Data Analysis.* Cambridge University Press, New York

Daley, R. and E. Barker 2000 *NAVDAS Source Book.* NRL Publication NRL/PU/7530-00-418.

Douglass, A. R., Schoeberl, M. R., Rood, R. B., and Pawson, S.	2003	Evaluation of transport in the lower tropical stratosphere in a global chemistry and transport model, *J. Geophys. Res.*, **108**, doi:10.1029/2002JD002696
Folland, G. B.	1992	*Fourier analysis and its applications.* Wadsworth & Brooks, Pacific-Grove, CA
Gaspari, G. and Cohn, S. E.	1999	Construction of correlation functions in two and three dimensions. *Q. J. R. Meteorol. Soc.*, **125**, 723–757
Hamilton, K., Hertzog, A., Vial, F., and Stenchikov, G.	2004	Longitudinal variation of the stratospheric quasi-biennial oscillation. *J. Atmos. Sci.*, **61**, 383–402
Hannan, E. J.	1970	*Multiple time series.* Wiley, New York
Hollingsworth, A. and Lönnberg, P.	1986	The statistical structure of short-range forecast errors as determined from radiosonde data. Part I: The wind field. *Tellus*, **38A**, 111–136
Holton, J. R.	1992	*An Introduction to Dynamic Meteorology.* Academic Press, New York
Klinker, E., Rabier, F., Kelly, G., Mahfouf, J.-F.	2000	The ECMWF operational implementation of four-dimensional variational assimilation. III: Experimental results and diagnostics with operational configuration. *Q. J. R. Meteorol. Soc.*, **126**, 1191–1215
Loève, M.	1963	*Probability Theory, 3rd ed.* Van Nostrand, Princeton
Lönnberg, P. and Hollingsworth, A.	1986	The statistical structure of short-range forecast errors as determined from radiosonde data, Part II: The covariance of height and wind errors. *Tellus*, **38A**, 137–161
Mahfouf, J.-F. and Rabier, F.	2000	The ECMWF operational implementation of four-dimensional variational assimilation. II: Experimental results with improved physics. *Q. J. R. Meteorol. Soc.*, **126**, 1171–1190
Ménard, R., Cohn, S. E., Chang, L.-P., and Lyster, P. M.	2000	Assimilation of stratospheric chemical tracer observations using a Kalman filter. Part I: Formulation. *Mon. Wea. Rev.*, **128**, 2654–2671
Parrish, D. F. and Derber, J. C.	1992	The National Meteorological Center's spectral statistical-interpolation analysis system. *Mon. Weather Rev.*, **120**, 1747–1763
Pawson, S. and Fiorino, M.	1998b	A comparison of reanalyses in the tropical stratosphere. Part 2: The quasi-biennial oscillation. *Climate Dyn.*, **14**, 645–658
Phillips, N. A.	1986	The spatial statistics of random geostrophic modes and first-guess errors. *Tellus* **38A**, 314–332
Rabier, F., Mc Nally, A., Andersson, E., Courtier, P, Undén, P., Eyre, J., Hollingsworth, A., and Bouttier, F.	1998	The ECMWF implementation of three dimensional variational assimilation (3D-Var). Part II: Structure functions. *Q. J. R. Meteorol. Soc.*, **124**, 1809–1830
Rabier, F., Järvinen, H, Klinker, E., Mahfouf, J.-F., and Simmons, A.	2000	The ECMWF operational implementation of four-dimensional variational assimilation. I: Experimental results with simplified physics. *Q. J. R. Meteorol. Soc.*, **126**, 1143–1170
Randel, W. J., Wu, F., Swinbank, R., Nash, J., and O'Neill, A.	1999	Global QBO Circulation Derived from UKMO Stratospheric Analysis. *J. Atmos. Sci.*, **56**, 457–474
Randel, W., Udelhofen, P., Fleming, E., Geller, M., Gelman, M., Hamliton, K., Karoly, D., Ortland, D., Pawson, S., Swinbank, R., Wu, F., Baldwin, M., Chanin, M-L., Keckhut, P., Labitzke, K., Remsberg, E., Simmons, A., and Wu, D.	2004	The SPARC Intercomparison of Middle-Atmosphere Climatologies. *J. Climate*, **17**, 986–1003

Yaglom, A. M. 1987 *Correlation Theory of Stationary and Related Random Functions, Vol. I: Basic Results*, Springer-Verlag, New York

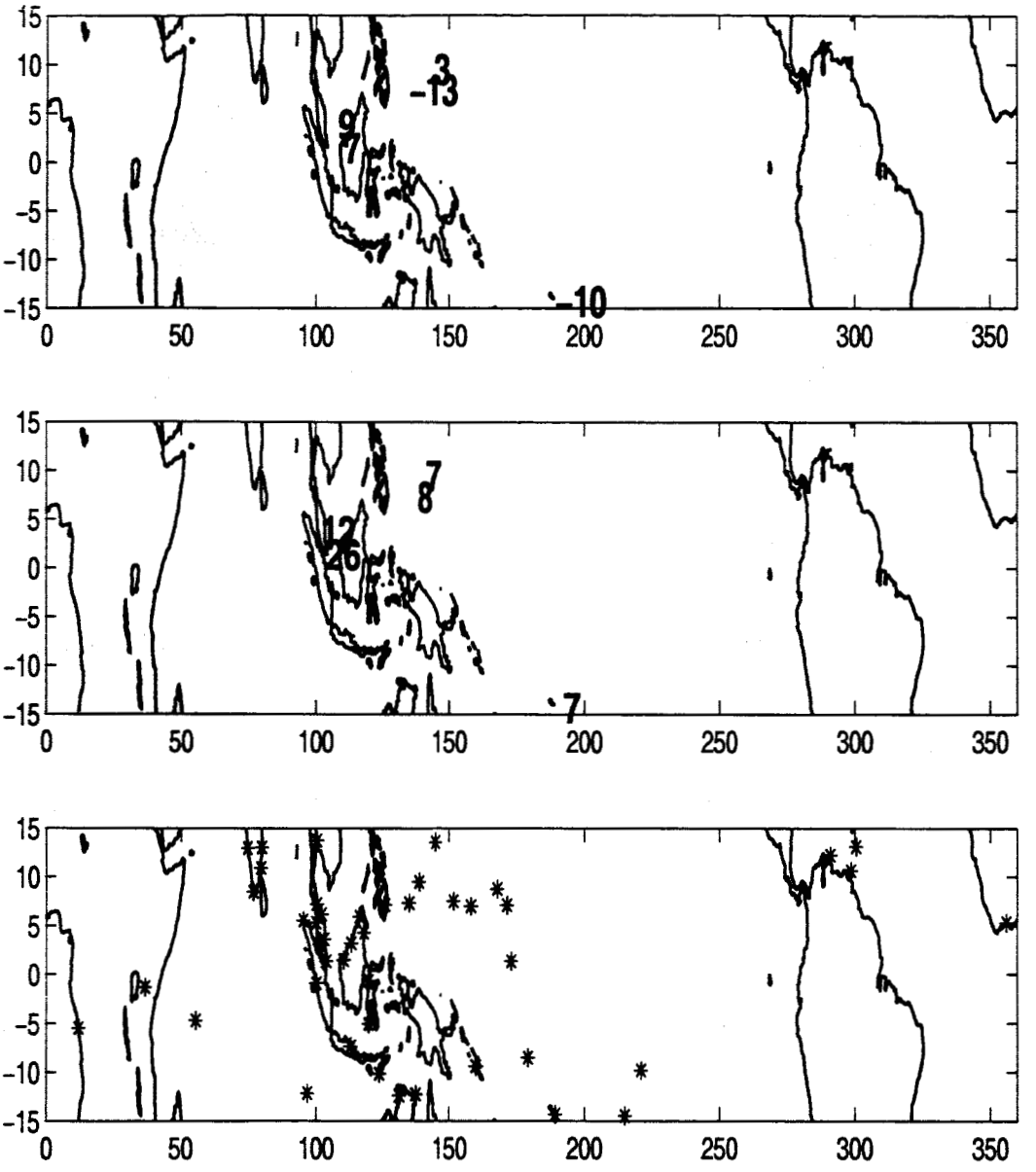

Figure 1. The top panel is average value of the 10 hPa zonal wind over Nov. 1991 at 0000 GMT, for all tropical radiosonde stations reporting 5 or more times in Nov. 1991. The 9 ms^{-1} value at 3.75° N, 102° E is the reporting frequency weighted average over the two stations at (3.1°, 101.65°) and (3.62°, 103.22°). The location (3.75°, 102°) is the center of the 2.5° × 4° lat-lon box used for the averaging. All other values are shown at the reporting station locations. The second panel is the total number of 10 hPa zonal wind reports at 00 GMT over Nov. 1991. The combined number of reports from (3.1°, 101.65°) and (3.62°, 103.22°) is 12, shown at (3.75°, 102°). The third (lowest) panel marks the location of all tropical radiosonde stations with 5 or more 50 hPa wind reports at 0000 GMT in Nov. 1991. Note the negative averages of -13 ms^{-1} at (7.33°, 134.48°) and -10 ms^{-1} at (−14.33°, 189.28°).

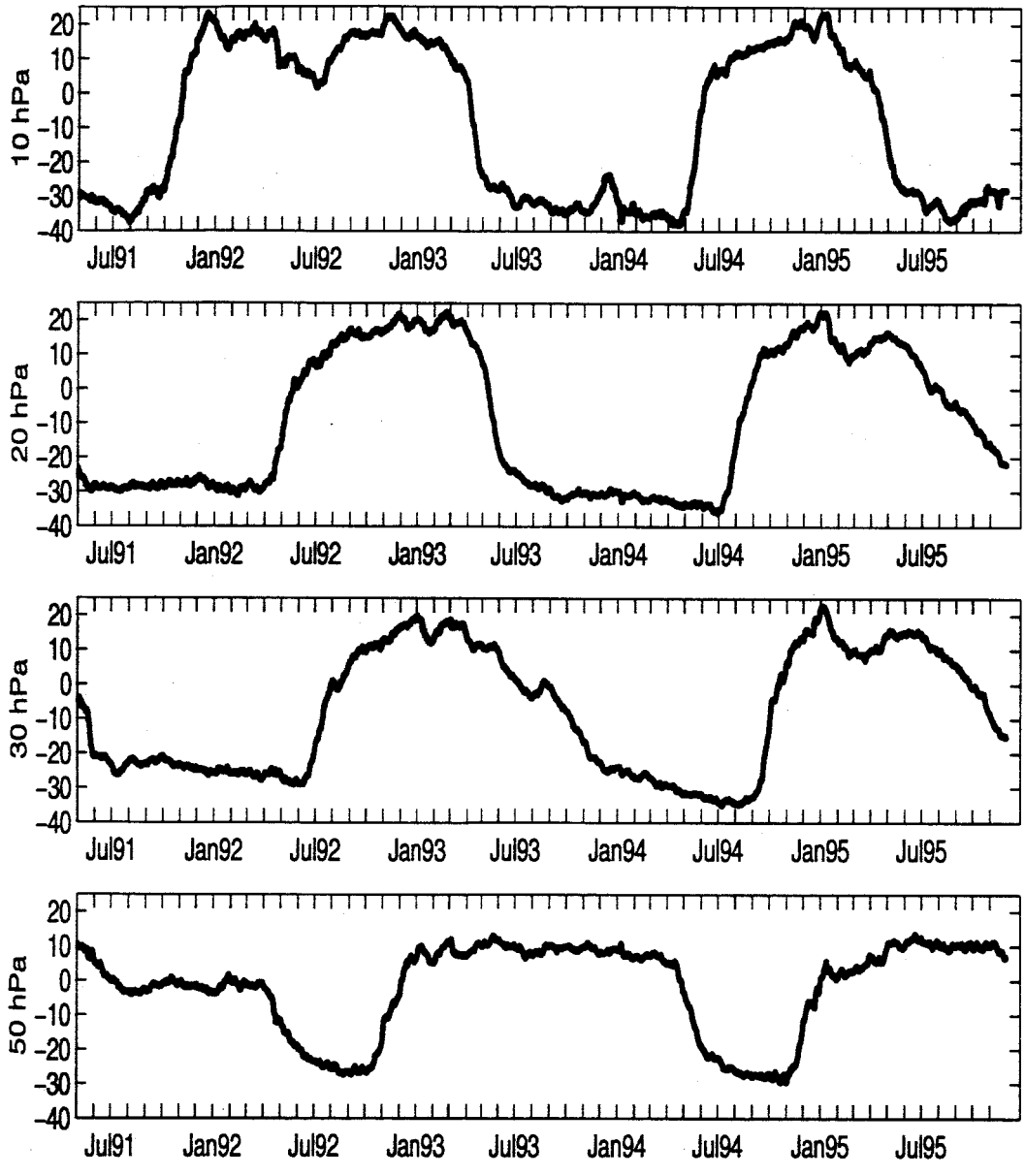

Figure 2. Ten day centered moving average of zonal wind radiosonde observations in ms^{-1} at the Singapore radiosonde.

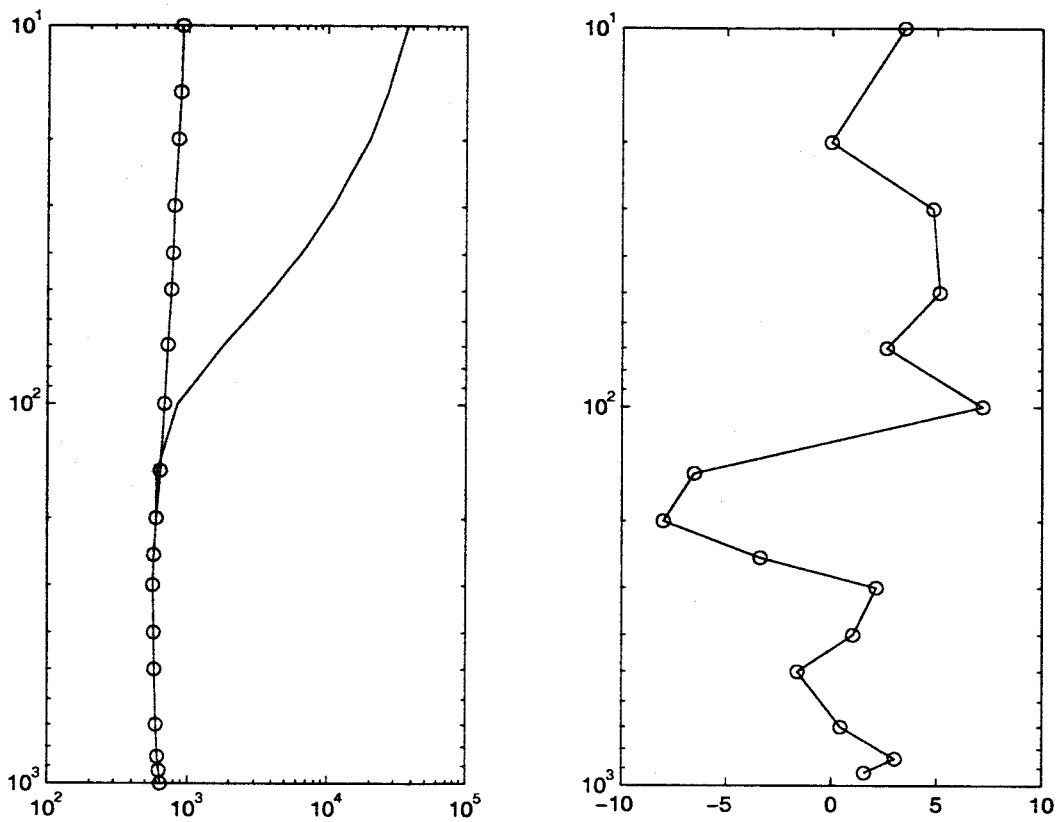

Figure 3. The left panel is the streamfunction length scales in models A and B, where the longer length scales are used in model A. The x-axis is the length scale in kilometers and the y-axis is pressure in hPa. The right panel is the observed-minus-forecast zonal wind in ms^{-1} (x-axis) at Singapore used in a static PSAS analysis to produce the analysis increments shown in Figs. 4 and 5.

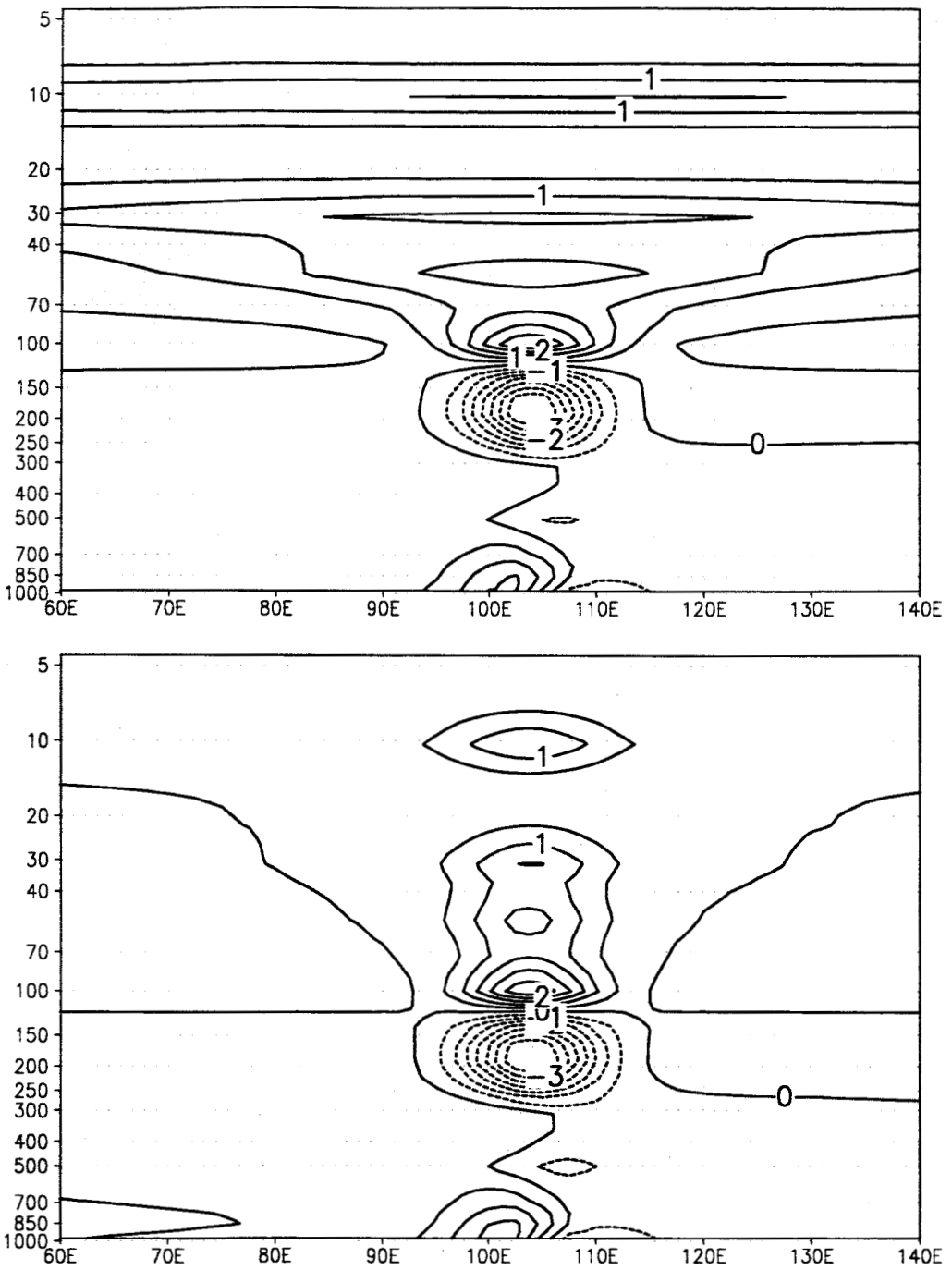

Figure 4. Zonal wind analysis increments at latitude 2° N in ms^{-1} from a static PSAS analysis using a single radiosonde profile at Singapore with observed-minus-forecast zonal winds shown in Fig. 3. The upper panel shows the increments due to model A. The lower panel shows the increments due to model B. The contour interval is .5 ms^{-1}.

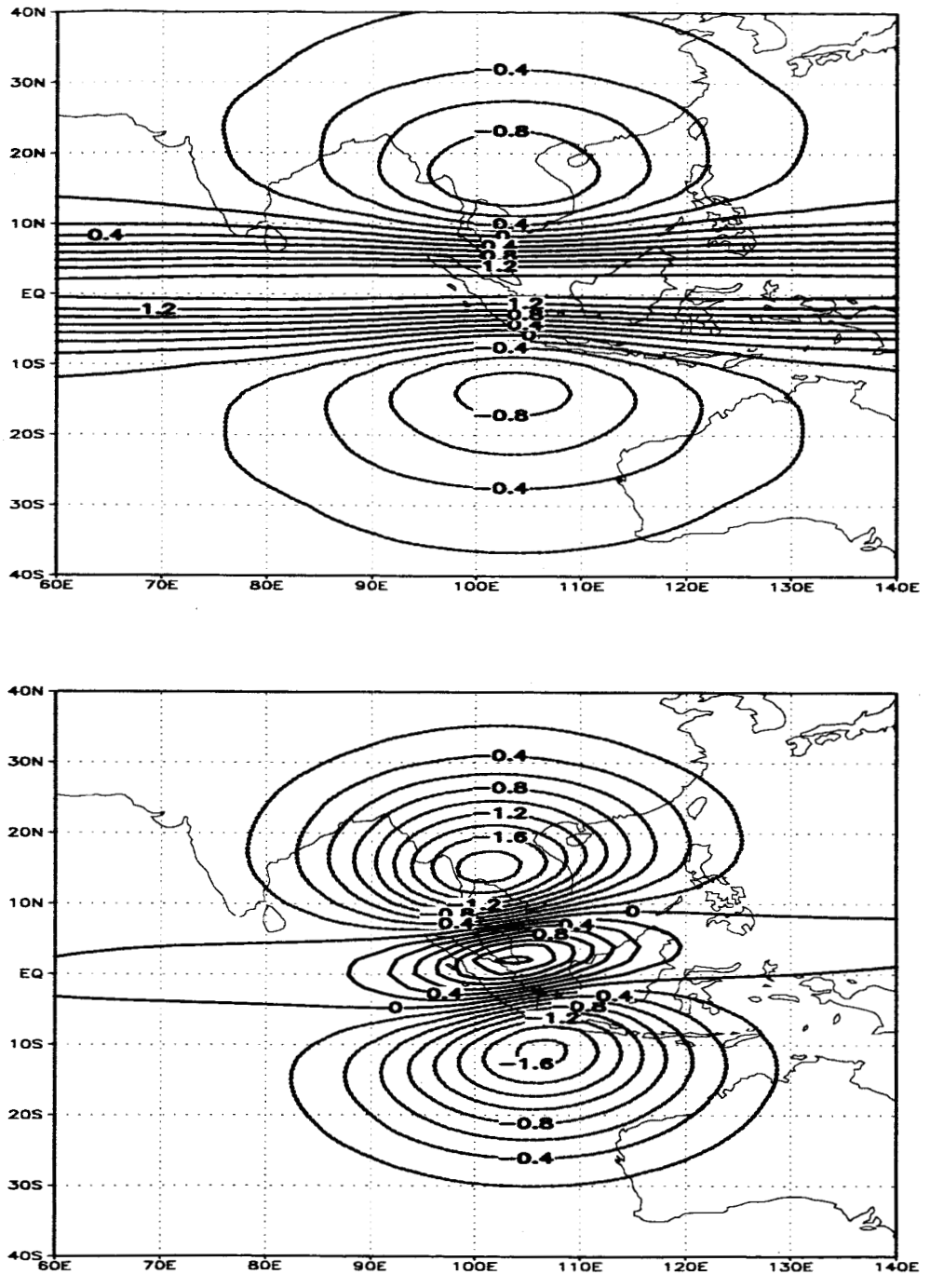

Figure 5. Zonal wind analysis increments at 10 hPa in ms^{-1} from a static PSAS analysis using a single radiosonde profile at Singapore with observed-minus-forecast zonal winds shown in Fig. 3. The upper panel shows the increments due to model A. The lower panel shows the increments due to model B. The contour interval is .2 ms^{-1}.

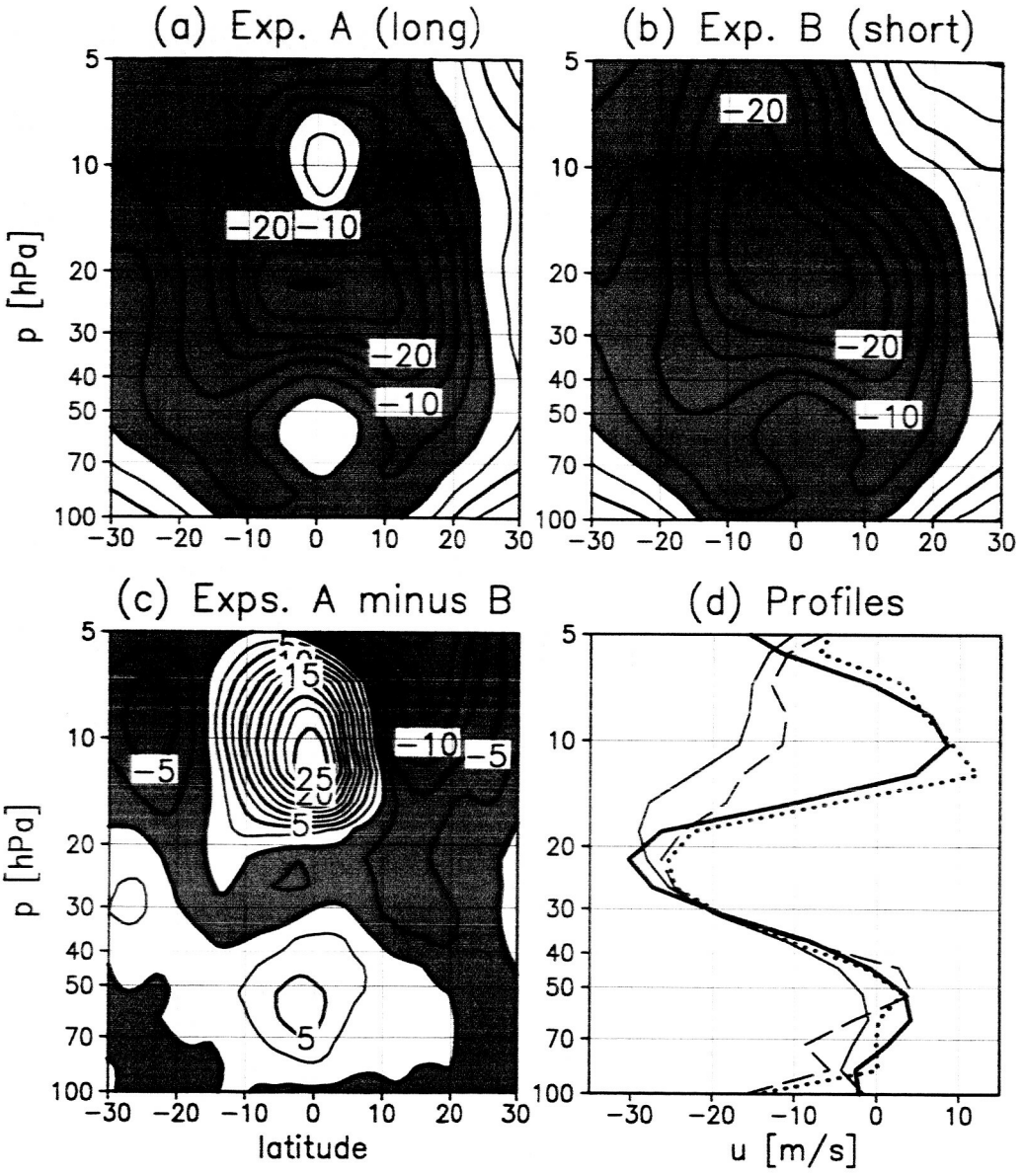

Figure 6. The upper panels show the longitudinally averaged zonal wind field in ms^{-1} at 00 GMT on 30 November 1991. Experiment A is shown on the left and Experiment B is shown on the right. The y-axis is pressure in hPa, the x-axis is latitude, and the contour interval is 10 ms^{-1}. The difference of the upper left and right panels is shown in the lower left panel with a contour interval of 5 ms^{-1}. Profiles of the zonal wind field in ms^{-1} near Singapore are shown in the lower right panel, where the x-axis is the zonal wind and the y-axis is pressure in hPa. The dotted (dashed) solid curve is the zonal wind for Exp. A (Exp. B) at latitude 1° N and longitude 103.75° E. The thick (thin) curve is the longitudinally averaged zonal wind for Exp. A (Exp. B) at latitude 1° N.

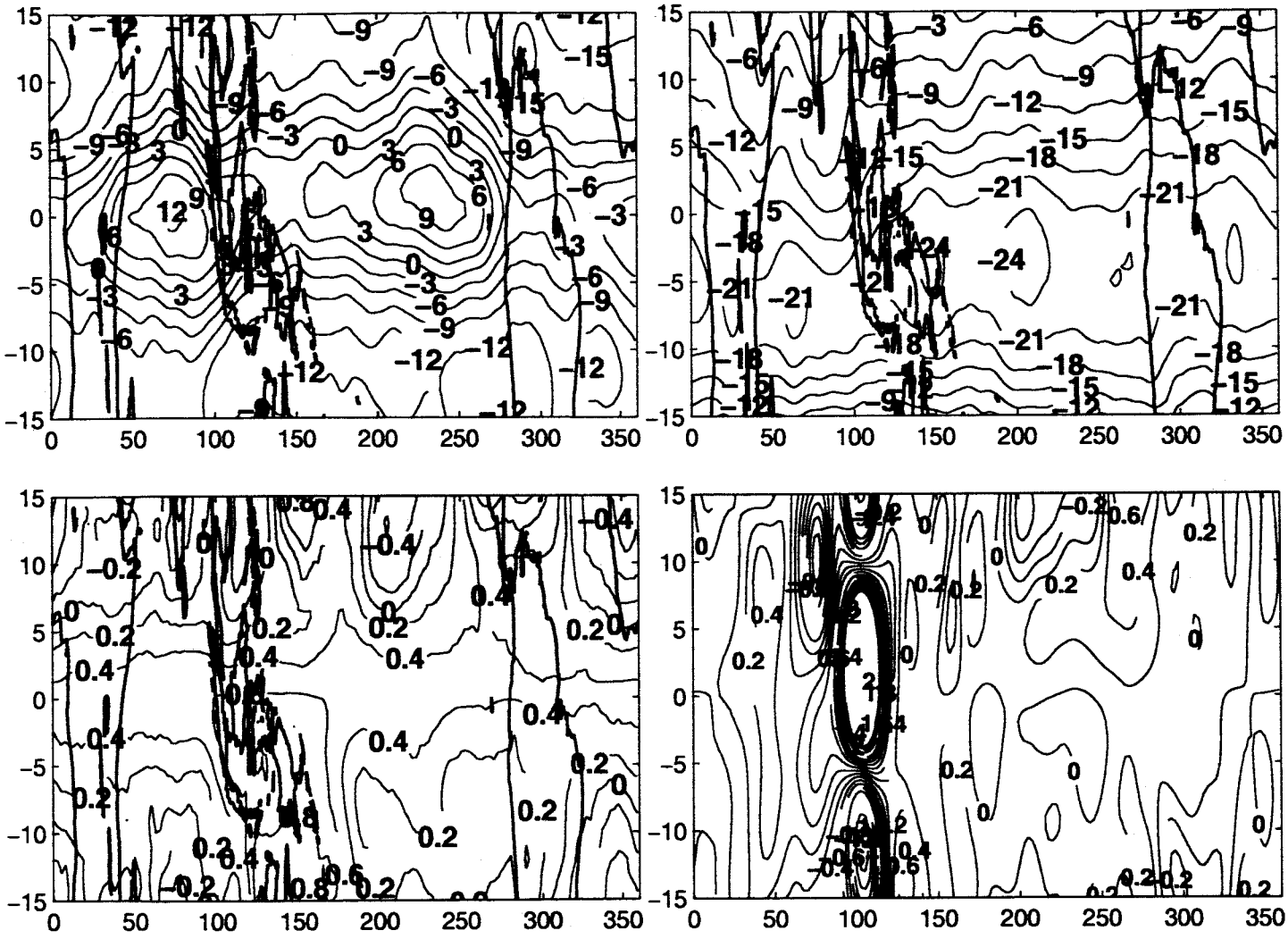

Figure 7. The monthly averaged zonal wind for Exp. A and B in ms^{-1} at 10 hPa at 00 GMT over November 1991 is shown in the upper two panels. The monthly averaged zonal wind analysis increments in ms^{-1} for Exp. A and B at 10 hPa at 00 GMT over November 1991 is shown in the lower two panels. The averages for Exp. A (Exp. B) are shown in the left (right) panels. The contour interval for the upper (lower) panels is 3 ms^{-1} (.2 ms^{-1}).

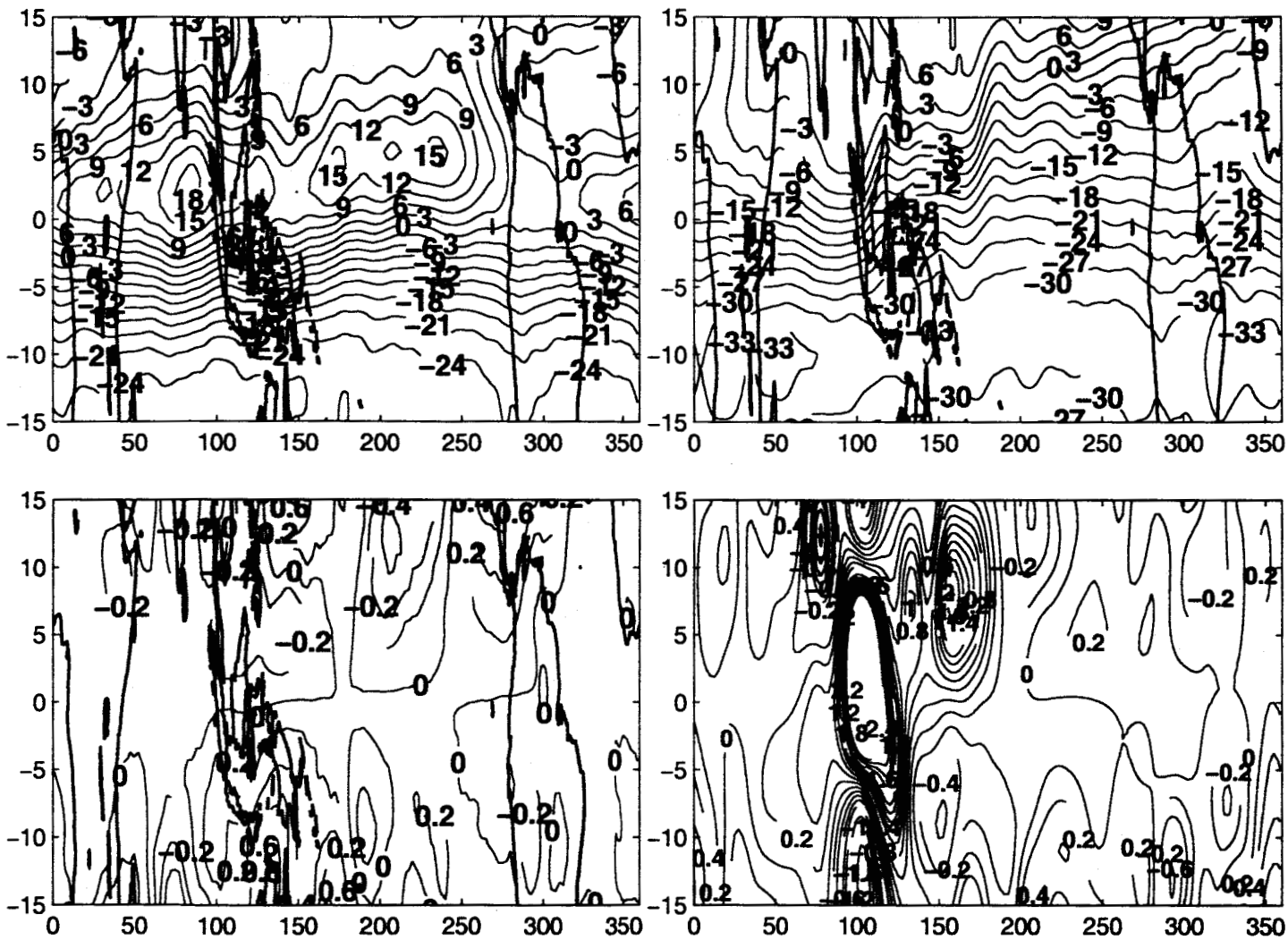

Figure 8. As in Fig. 7, for January 1992.

Popular Summary

Construction of Covariance Functions with Variable Length Fields

Gregory Gaspari, Stephen E. Cohn, Jing Guo, Steven Pawson

Geophysical data assimilation involves using principles of estimation theory to merge diverse observations and short-term model predictions to yield so-called "optimal" analyses of the system state. The optimization in assimilation is effected using the best possible weighting of model errors against observation errors. The ability to accurately determine this weighting is arguably one of the least well understood aspects of the assimilation, due primarily to the diverse range of conditions encountered in the atmosphere. For this reason, the quality of an assimilation is typically evaluated experimentally, based on the geophysical response to perturbations to one or more of the following: the statistical analysis, the observing system, and the model. The former two components are interrelated in the sense that covariance modeling assumptions determine the spatio-temporal influence of observations through so-called "analysis increments" that act to iteratively correct the model state over the course of the assimilation. In meteorological applications, analysis increments are typically produced using background and observation error covariance models applied to determine the spatio-temporal influence of a diverse set of in-situ, or "point" measurements (e.g., balloon soundings, aircraft observations) with a diverse set of satellite observations (e.g., space-based radiance data). Effective analysis increments should cause high-quality observations to be distributed over length scales appropriate to the region of the atmosphere, and appropriate for the spatio-temporal data coverage. Geophysical length scales differ widely between the atmospheric boundary layer, the free troposphere and the stratosphere. A practical determination of the correlation length scale should account for these differences, while also accounting for differences between data-dense and data-poor regions of the atmosphere.

This paper presents new theoretical developments for a formal mechanism of incorporating geographically- and height-dependent length scales in the assimilation, extending earlier theoretical developments of Gaspari and Cohn (1999).

An application is presented for the assimilation of tropical wind observations, where the length scale in the sparsely observed stratosphere is much longer than that in the more densely observed troposphere. It is demonstrated, using the GMAO's GEOS-4 data assimilation system, that using a zonally extended length scale in the tropical stratosphere leads to a much more realistic quasi-biennial oscillation than with the shorter length scales used in the standard system.